Circularly Polarized V-band Orthomode Transducer

Shoukry Shams, *Senior Member, IEEE*, Abdullah Muhammad Mahfouz, Mahmoud Elsaadany, *Senior Member, IEEE*, Mohamed A. Moharram Hassan, Ghyslain Gagnon, *Member, IEEE* and Ahmed A Kishk, *Life Fellow, IEEE*

***Abstract*—A compact septum-based orthomode transducer (OMT) is designed to provide dual circularly polarized states for horn antennas. The OMT is back-fed by two rectangular ports separated by a stepped tapered septum from thick to thin walls towards the common port. The OMT covers 16.7% fractional bandwidth in the V-band (55 - 65 GHz), which coincides with the fifth generation and beyond (5GB) communications standards and inter-satellite communications. The OMT performance is evaluated by measuring the back-to-back (BTB) scattering parameters. Measured insertion loss (IL) is below 1.3 dB, whereas the isolation between the rectangular ports remains beyond 17 dB in the operating band.**

***Index Terms*—Orthomode transducer (OMT), antenna feed, mmWave components, septum polarizer, satellite communications, PLF**

I. Introduction

SHORT range communication in the wide license-free bandwidth (57 - 66) GHz promotes numerous applications such as wireless local and personal area networks [1], high definition video streaming [2]. The antenna polarization is crucial as the signal attenuation is high, around 60 GHz band [3]. Circular polarized (CP) antennas enhance system capacity through a significant reduction of the multipath effects in wireless channels compared to linearly polarized (LP) antennas with similar radiation characteristics [4], [5]. Moreover, polarization diversity can be achieved using orthomode transducers (OMTs), which can simultaneously receive or transmit CP waves with a different sense of rotation. Accordingly, a widely used technique is integrating CP antennas and OMTs [6]–[10].

Various topologies were designed to create orthogonal and quadrature-phase field components such as inserting transverse irises or periodic grooves along the propagation direction [11]–[13]. Besides, splitting a regular shape waveguide port into two identical ports using a metallic graded septum provides such field decomposition as well; and these waveguides are called septum OMTs. The discrimination between CP waves of a different sense of rotation is accomplished by the metallic stepped septum parallel to the propagation direction in the common port. The output ports usually have a standard interface such as a rectangular or double ridge waveguide [14]–[16]. On the other hand, the common port usually has a non-standard interface connected to a horn antenna. Although square and circular waveguides are frequently used as common ports [14], an equilateral triangular waveguide is recently used due to its significant improvement of the fractional bandwidth (FBW) in the W-band [17]. Changing septum steps' height, length, and thickness have considerable effects on the OMT performance. A constant thickness septum has been designed and tested in Q- and K-bands [14]. In contrast, stepped-thickness septum OMT was designed for X-band to increase the isolation between the output ports [18].

In this letter, we adopt a circular waveguide septum polarizer with a thick stepped-thickness septum to extend the operating bandwidth to cover 55 to 65 GHz (16.7% FBW). The letter is organized as follows. A detailed design procedure of the proposed OMT is explained in Section II. The experimental validation and results discussion come in Section III. A comparison is carried out between the proposed OMT and the previously published OMTs in section IV, followed by a brief list of the article outcomes in section V.

Shoukry Shams is with the ECE Department, Concordia University (e-mail: shoukry.shams@ieee.org).

Abdullah Muhammad Mahfouz is with the EE Department, Faculty of Engineering, Assiut University (e-mail: eng.mahfouz1992@aun.edu.eg).

Mahmoud Elsaadany and Ghyslain Gagnon are with EE Department, École de technologie supérieure

Mohamed A. Moharram is with the EECE Department, Faculty of Engineering, Cairo University

Ahmed A Kishk is with the ECE Department, Concordia University

II. Proposed Design Methodology & Description

The design process of a septum OMT can be summarized in two steps: First, studying the dispersion characteristics of the common port and one of the output ports, which determines the available BW. The second step is to optimize the septum parameters to achieve the objective specifications for both CP purity and isolation between the output ports.

A. Design Procedure

Since the OMT is intended 60 GHz band (55-65 GHz), the dimensions of all ports must assure that the objective band lies in a common frequency range that suits all ports. As for the identical ports, the objective band must be confined between the cutoff frequencies of the dominant mode and the following higher-order mode. Thus, the suitable candidate interface is the standard WR15 rectangular waveguide with a cross-section of 148×74 mil^2. Thus the dominant mode cutoff frequency of the WR15 is 39.9 GHz, whereas the following high-order modes are TE_{20} and TE_{01}, with a cutoff frequency of 79.8 GHz.

Alternatively, the actual common port dimensions are taken close to the WR15 standard width to assure a common frequency range between the common port and the other two ports. A quasi-square opening terminates the septum with dimensions of 135.9×118 mil^2. These opening dimensions ensure that the first two modes' cutoff frequencies are below 55 GHz, while the third cutoff is above 65 GHz. The three successive modes of that opening are TE_{10}, TE_{01}, and TE_{11} modes, which correspond to cutoff frequencies of 46.5, 50, and 66.3 GHz, respectively. A rectangular-to-circular waveguide transition is connected to the quasi-square opening in order

This article has been accepted for publication in IEEE Antennas and Wireless Propagation Letters. This is the author's version which has not been fully edited and content may change prior to final publication. Citation information: DOI 10.1109/LAWP.2022.3201002

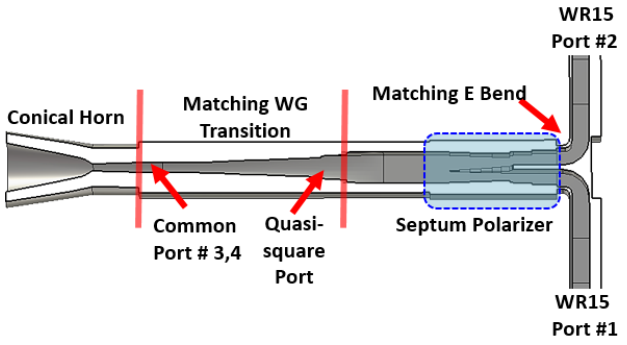

(a)

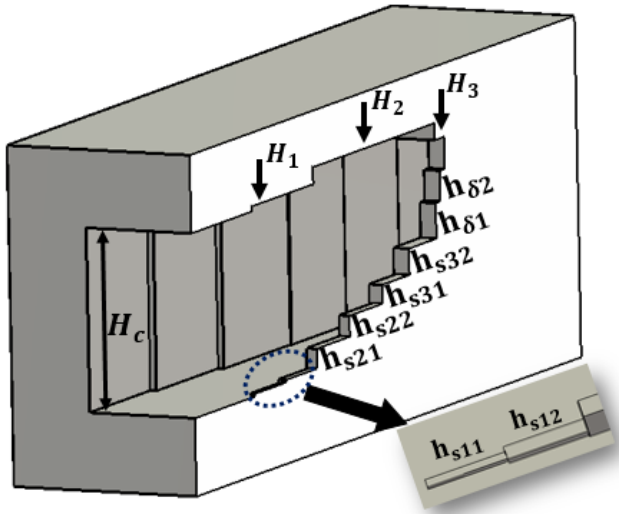

(b)

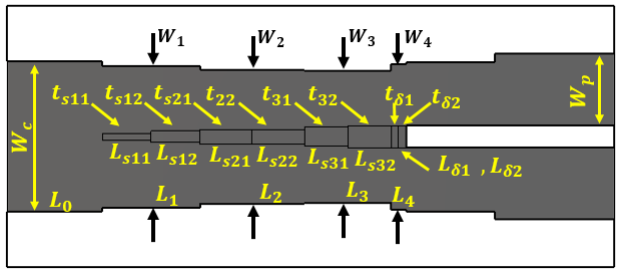

(c)

Fig. 1. Cross-sectional view of a conical horn integrated with the proposed OMT with dimensions.(a) Full assembly. (b) Cross-sectional OMT side view. (c) Cross-sectional OMT top view.

to obtain a symmetric port shape, which ensures identical dispersion behavior of both degenerated modes, as illustrated in Fig. 1a. The circular port diameter is 140 mil corresponding to the dominant mode cutoff frequency (TE_{11}) of 49.44 GHz, whereas the successive mode is TM_{01} with a cutoff frequency of 64.5 GHz. Therefore, both modes of the quasi-square opening are represented by the dominant circular port TE_{11} mode with two orthogonal orientations.

The proposed OMT includes a septum of 6 steps with different thicknesses to provide a graded transition from the septum to the common port. The lengths of the septum steps are initially assigned to be about $0.25\lambda_g$ at the mid-band frequency. The septum is optimized using Nelder Mead simplex algorithm integrated inside CST microwave studio suite to maintain the isolation and the return loss (RL) above 20 dB and keep the AR below 1 dB. The optimized dimensions of the septum are listed in Table I.

TABLE I
DETAILED DIMENSIONS OF THE PROPOSED OMT IN MILS

Septum dimensions				General dimensions			
t_{s11}	6	L_{s31}	38.8	H_c	118	H_1	121.3
t_{s12}	10	L_{s32}	38.8	W_c	135.9	H_2	132.1
t_{s21}	13	$L_{\delta 1}$	6.8	W_p	74	H_3	121.3
t_{s22}	13	$L_{\delta 2}$	6.8	L_0	85.8		
t_{s31}	17	h_{s11}	1.7	L_1	87.5		
t_{s32}	20	h_{s12}	1.7	L_2	94.2		
$t_{\delta 1}$	20	h_{s21}	12.7	L_3	77.6		
$t_{\delta 2}$	20	h_{s22}	13.4	L_4	13.5		
L_{s11}	43.8	h_{s31}	12.1	W_1	127.9		
L_{s12}	43.8	h_{s32}	16.8	W_2	120.7		
L_{s21}	47.1	$h_{\delta 1}$	22.7	W_3	118.9		
L_{s22}	47.1	$h_{\delta 2}$	19.6	W_4	106.1		

B. Proposed OMT Simulation Results

The simulation results of the optimized OMT are illustrated in Fig. 2. The isolation between the identical ports is below -25 dB. Moreover, the reflection coefficient of the rectangular port is below -15 dB. The AR is calculated using common Port simulated fields through the following equation [19]

$$AR = \sqrt{\frac{|S^c_{31}|^2 + |S^c_{41}|^2 + |S^c_{43}|^2}{|S^c_{31}|^2 + |S^c_{41}|^2 - |S^c_{43}|^2}}, \qquad |S^c_{43}|^2 = \sqrt{|S^c_{31}|^4 + |S^c_{41}|^4 + 2|S^c_{31}|^2|S^c_{41}|^2 cos(2\Delta\phi^c_{43})} \tag{1}$$

where S^c_{31} and S^c_{41} define the virtual two ports corresponding to TE_{10} and TE_{01}, respectively, of the common port. $\Delta\phi^c_{43} = \phi^c_{41} - \phi^c_{31}$, which represents the phase difference between the S^c_{31} and S^c_{41}.

Furthermore, the OMT is simulated while a conical horn is terminating it to investigate the antenna loading effect on the OMT performance. The impedance matching and isolation after loading become less than -11 dB and -20 dB, respectively. In addition, the AR is calculated using the degenerated fields on the conical horn aperture and follows the same profile as the OMT AR, as shown in Fig. 2b. The far-field AR is also calculated using a far-field monitor at $\theta = 0^o$ and compared to the OMT AR for the entire band to verify the correctness of the calculated AR using the near-fields on the horn aperture. Moreover, the conical horn radiated fields are plotted in $\phi = 0^o$ and $\phi = 90^o$ azimuthal planes, as illustrated in Fig. 3a, Fig. 3b, Fig. 3c, and Fig. 3d. Furthermore, the AR is plotted in 5 various azimuthal plane cuts versus $\theta-$ in the maximum radiation region at the mid-band frequency, as shown in Fig.3e. In addition, the co-pol and x-pol gain are plotted versus frequency at $\theta = 0^o-$, as illustrated in Fig. 3f.

III. EXPERIMENTAL VERIFICATION AND DISCUSSION

Two OMT units are fabricated using MATSUURA computer numerical control (CNC) milling machine with an accuracy of

This article has been accepted for publication in IEEE Antennas and Wireless Propagation Letters. This is the author's version which has not been fully edited and content may change prior to final publication. Citation information: DOI 10.1109/LAWP.2022.3201002

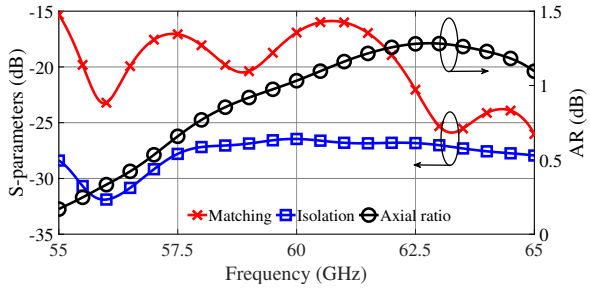

(a)

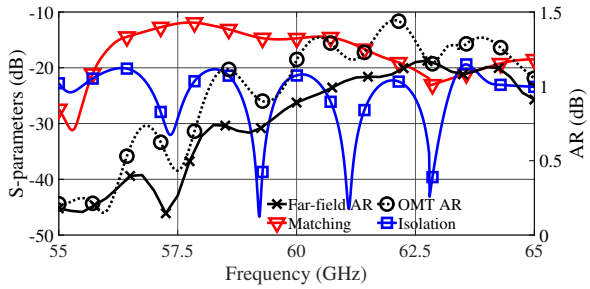

(b)

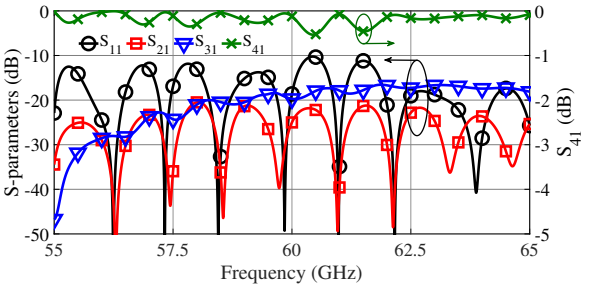

(c)

Fig. 2. OMT simulated results associated with the optimized dimensions. (a) Impedance matching, Isolation & AR for a non-loaded OMT, (b) Impedance matching, Isolation & AR with a conical horn load, and (c) Simulated BTB scattering parameters

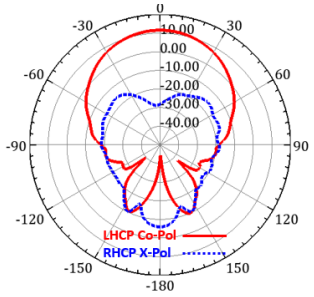

(a)

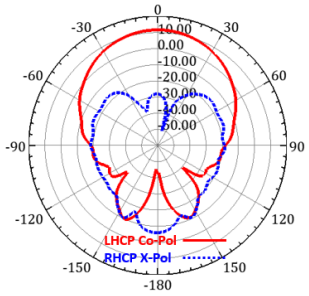

(b)

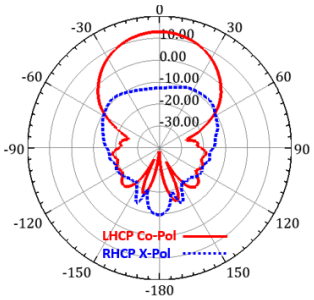

(c)

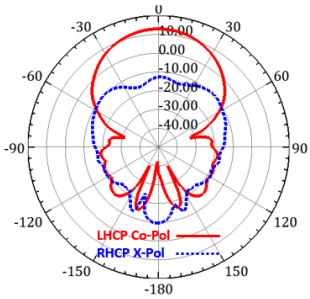

(d)

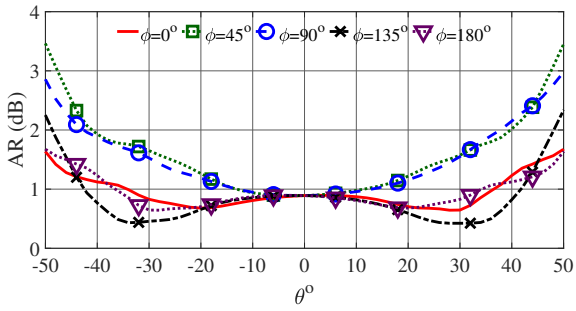

(e)

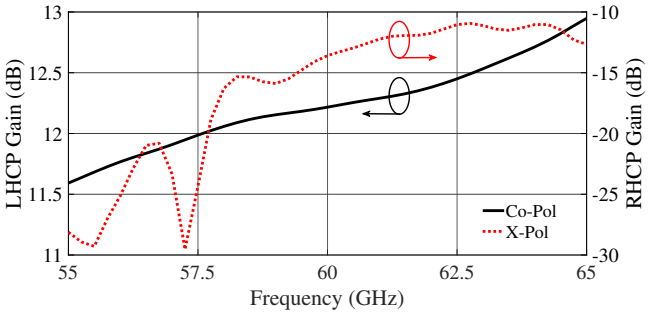

(f)

Fig. 3. Far-field radiation patterns. (a) $\phi = 0^0$ @ 55 GHz, (b) $\phi = 90^0$ @ 55 GHz, (c) $\phi = 0^0$ @ 65 GHz, (d) $\phi = 90^0$ @ 65 GHz, (e) AR versus θ at different azimuthal plane cuts @ 60 GHz, and (f) Co- and X-pol gain levels vs. frequency @ $\theta = 0$

± 0.5 mil, as shown in Fig. 4a. Both OMT units are connected in the back-to-back (BTB) configuration and tested, as shown in Fig. 4b. Therefore, the resultant structure represents a 4-port network in which the compatible two ports are coupled while the other two ports are isolated. The measured scattering parameters versus frequency of the overall structure are illustrated and compared to the simulated curves in Fig. 5a and Fig. 5b. The maximum value of the reflection coefficient is around -14 dB due to the loading effect in the BTB configuration. The IL is below 1.3 dB, whereas the isolation coefficient are above 19 dB for the whole operating band. The deviation between the simulated and measured responses is due to the fabrication tolerances, especially with the small dimensions in such frequency bands. However, the measured isolation and impedance matching responses are still below -14 dB.

IV. Proposed OMT Performance Evaluation

Different technologies have been used for designing OMTs in various frequency bands. However, waveguide-based OMTs [12], [17], [20] can handle larger power than printed OMTs [6], [8], [9], [13]. In addition, the associated antenna with the SIW OMT has almost either a printed H-plane sector horn [6], [8] or an array of patches [9] with lower gain compared to conical or pyramidal horns.

From the BW perspective, most of the presented designs

This article has been accepted for publication in IEEE Antennas and Wireless Propagation Letters. This is the author's version which has not been fully edited and content may change prior to final publication. Citation information: DOI 10.1109/LAWP.2022.3201002

TABLE II
TABLE OF COMPARISON

Ref	Technology	FBW(%) Freq. range (GHz)	AR (dB) below	IL (dB) below	RL (dB) above	ISO (dB) above	Approximate size	Compatibility with horn antenna
[6]	SIW	4.7 83-87	0.98	N/A	10	25	$92.4\lambda^3$ @85GHz	✓
[8]	SIW	30 22-29.8	3	N/A	10	N/A	$1.9\lambda^3$ @26GHz	✓
[9]	SIW	0.71 35.3-35.55	3	N/A	10	N/A	$0.02\lambda^3$ @35.4GHz	✗
[12]	Mono-groove	10.5 54-60	2.2	N/A	10	15 sim.	$1.84\lambda^3$ @57GHz	✓
[13]	SIW& septum	7.9 27.85 - 30.15	3	1.6	20	10	$0.026\lambda^3$ @29GHz	✓
Present	septum	16.7 meas. 55-65	1.3 sim.	1.3 meas.	14 meas.	20 meas.	$0.76\lambda^3$ @60GHz	✓

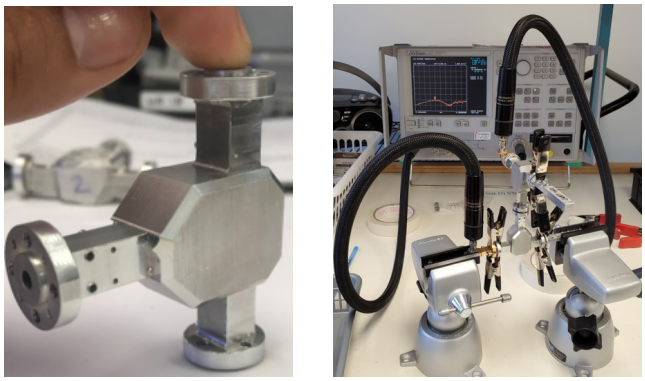

(a) (b)

Fig. 4. Photos of (a) Fabricated OMT and (b) Measurement setup of the BTB configuration.

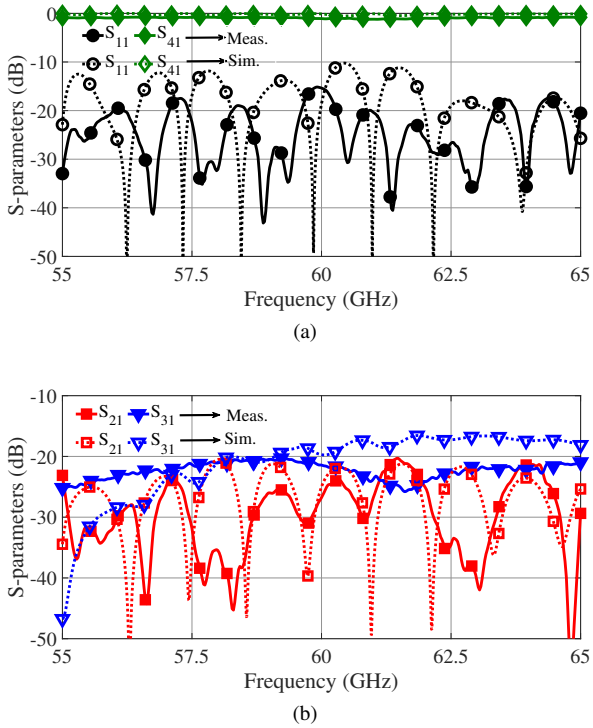

(a)

(b)

Fig. 5. Measured and simulated S-parameters of the BTB configuration. (a) Reflection and transmission coefficients S_{11} and S_{41} and (b) S_{21} and S_{31}.

provide a bandwidth limited to 10% or below [6], [9], [12], [13]. However, some designs achieve a wide-band with poor matching and isolation levels [8]. On the other hand, some designs have exceeded 30% bandwidth with a triangular-shaped common port, which is unsuitable for integration with conical/pyramidal horn antennas [17]. Other designs achieved slightly more than 15% FBW with featured AR and RL such as [7], [20]. However, they focused only on the OMT center section without studying the OMT performance in the actual configuration when it is connected to the bends for achieving dual polarization states.

The simplicity of design and fabrication is clearly revealed in [12], which uses a compact cylindrical waveguide section with an outward protruding groove cascaded by a conical horn antenna. However, we can deduce that the FBW, isolation, and impedance matching still need some improvements. The performance evaluation is summarized in Table II, where we included only the complete designs that have two distinct ports for the two orthogonal polarization states. In addition, we omitted all designs that are not compatible with horn antennas.

As for the proposed OMT structure, it presents a valuable compromise between the OMT aspects. Its size lies in the same range of the other counterparts with overall septum length does not exceed 1.39λ @ 60 GHz . Moreover it is presented in a full configuration setup taking into account the practical considerations of the bends and the horn antenna. Furthermore, it provides a 16.7% FBW, which is wider than or equal to most of the previously published OMTs with a relatively satisfactory BTB impedance matching level of 14 dB. Besides, the BTB isolation between the output ports is above 20 dB, assuring better CP purity.

V. CONCLUSION

A V-band orthomode transducer has been designed, fabricated, and experimentally validated to cover 55 to 65 GHz frequency range. The insertion loss of the back-to-back configuration remained below 1.3 dB, whereas the impedance matching and the isolation are maintained below -14 dB due to utilizing a graded thickness waveguide in the common port, which has enhanced the impedance matching.

REFERENCES

[1] M. S. Rabbani and H. Ghafouri-Shiraz, "Improvement of microstrip patch antenna gain and bandwidth at 60 GHz and X bands for wireless applications," *IET Microwaves, Antennas & Propagation*, vol. 10, no. 11, pp. 1167–1173, April 2016.

[2] C. J. Hansen, "WiGiG: Multi-gigabit wireless communications in the 60 GHz band," *IEEE Wireless Communications*, vol. 18, no. 6, pp. 6–7, Dec. 2011.

[3] J. Zhu, S. Liao, Y. Yang, S. Li, and Q. Xue, "60 GHz dual-circularly polarized planar aperture antenna and array," *IEEE Transactions on Antennas and Propagation*, vol. 66, no. 2, pp. 1014–1019, Dec. 2017.

[4] F. A. Dicandia, S. Genovesi, and A. Monorchio, "Analysis of the performance enhancement of MIMO systems employing circular polarization," *IEEE Transactions on Antennas and Propagation*, vol. 65, no. 9, pp. 4824–4835, Sept. 2017.

[5] T. S. Rappaport and D. A. Hawbaker, "Wide-band microwave propagation parameters using circular and linear polarized antennas for indoor wireless channels," *IEEE Transactions on Communications*, vol. 40, no. 2, pp. 240–245, Feb. 1992.

[6] H. Jin, Y. M. Huang, H. Jin, and K. Wu, "E-band substrate integrated waveguide orthomode transducer integrated with dual-polarized horn antenna," *IEEE Transactions on Antennas and Propagation*, vol. 66, no. 5, pp. 2291–2298, Mar. 2018.

[7] S. Piltyay, A. Bulashenko, and I. Demchenko, "Waveguide iris polarizers for Ku-band satellite antenna feeds," *Journal of Nano- and Electronic Physics*, 2020.

[8] Y.-X. Zhang, Y.-C. Jiao, and L. Zhang, "Wideband inhomogeneous-polarizer loaded circularly polarized SIW horn antenna for broadband millimeter-wave applications," *IEEE Antennas and Wireless Propagation Letters*, vol. 18, no. 7, pp. 1448–1452, May 2019.

[9] W. Li, X. H. Tang, and Y. Yang, "A ka-band circularly polarized substrate integrated cavity-backed antenna array," *IEEE Antennas and Wireless Propagation Letters*, vol. 18, no. 9, pp. 1882–1886, Aug. 2019.

[10] Y. Cai, Y. Zhang, Z. Qian, W. Cao, and S. Shi, "Compact wideband dual circularly polarized substrate integrated waveguide horn antenna," *IEEE Transactions on Antennas and Propagation*, vol. 64, no. 7, pp. 3184–3189, July 2016.

[11] N. Yoneda, R. Miyazaki, I. Matsumura, and M. Yamato, "A design of novel grooved circular waveguide polarizers," *IEEE Transactions on Microwave Theory and Techniques*, vol. 48, no. 12, pp. 2446–2452, Dec. 2000.

[12] N. Luo, X. Yu, G. Mishra, and S. K. Sharma, "A millimeter-wave (V-band) dual-circular-polarized horn antenna based on an inbuilt monogroove polarizer," *IEEE Antennas and Wireless Propagation Letters*, vol. 19, no. 11, pp. 1933–1937, Aug. 2020.

[13] K. Al-Amoodi, R. Mirzavand, M. M. Honari, J. Melzer, D. G. Elliott, and P. Mousavi, "A compact substrate integrated waveguide notched-septum polarizer for 5G mobile devices," *IEEE Antennas and Wireless Propagation Letters*, vol. 19, no. 12, pp. 2517–2521, Nov. 2020.

[14] F. F. Dubrovka, S. I. Piltyay, R. R. Dubrovka, M. Lytvyn, and S. Lytvyn, "Optimum septum polarizer design for various fractional bandwidths," *Radio Electronics and Communications Systems*, vol. 63, no. 1, pp. 15–23, Jan. 2020.

[15] M. A. Abdelaal, S. I. Shams, M. A. Moharram, M. Elsaadany, and A. A. Kishk, "Compact full band OMT based on dual-mode double-ridge waveguide," *IEEE Transactions on Microwave Theory and Techniques*, vol. 66, no. 6, pp. 2767–2774, April 2018.

[16] M. A. Moharram, A. Mahmoud, and A. A. Kishk, "A simple coaxial to circular waveguide OMT for low-power dual-polarized antenna applications," *IEEE Transactions on Microwave Theory and Techniques*, vol. 66, no. 1, pp. 109–115, Aug. 2017.

[17] B. Deutschmann and A. F. Jacob, "Broadband septum polarizer with triangular common port," *IEEE Transactions on Microwave Theory and Techniques*, vol. 68, no. 2, pp. 693–700, Feb. 2020.

[18] F. Dubrovka, S. Piltyay, O. Sushko, R. Dubrovka, M. Lytvyn, and S. Lytvyn, "Compact X-band stepped-thickness septum polarizer," in *2020 IEEE Ukrainian Microwave Week (UkrMW)*, pp. 135–138, Nov. 2020.

[19] C. A. Balanis, *Antenna theory: analysis and design*. John Wiley & Sons, pp. 68-69, fourth ed., 2015.

[20] N. Nikolic, A. Weily, I. Kekic, S. L. Smith, and K. W. Smart, "A septum polarizer with integrated square to circular tapered waveguide transition," in *2018 IEEE International Symposium on Antennas and Propagation & USNC/URSI National Radio Science Meeting*, pp. 725–726, Jan. 2019.